


Matrix metalloproteinases are key targets of acupuncture in the treatment of ulcerative colitis

Rui-Bin Zhang*, Long-Cong Dong*, Qin Huang, Yuan Shen, Hong-Ying Li, Shu-Guang Yu and Qiao-Feng Wu 

Acupuncture and Tuina College, Chengdu University of Traditional Chinese Medicine, Chengdu 610075, China

*These authors contributed equally to this paper.

Corresponding authors: Shu-Guang Yu. Email: ysg@cducm.edu.cn; Qiao-Feng Wu. Email: wuqiaofeng@cducm.edu.cn

Impact statement

As a traditional Chinese medicine therapy, acupuncture has been used to treat ulcerative colitis (UC) for many years and has achieved good outcomes. However, the targets and mechanisms of acupuncture are still unclear. Through the establishment of an animal model of acupuncture, combined with full transcriptome data sequencing and bioinformatics analysis, we identified matrix metalloproteinases (MMPs) as key targets of acupuncture therapy for UC. We verified the transcriptome sequencing results by quantitative real-time polymerase chain reaction and western blot and immunohistochemical detection of proteins related to the intestinal barrier (Claudin-1, ZO-1, and Occludin). We also performed gene set enrichment and alternative splicing analyses and found that the metabolism of xenobiotics, sulfur compounds, and monocarboxylic acids are possible upstream targets, all of which supported biological processes related to MMPs. Therefore, we reasoned that acupuncture treatment of UC involved inhibition of MMPs, which this provides a theoretical and experimental basis to explain its therapeutic efficacy.

Abstract

The aim of this study was to elucidate the key targets of acupuncture in the colon of ulcerative colitis (UC) mice model using full-length transcriptome sequencing. 2.5% dextran sodium sulfate (DSS)-induced colitis mice were treated with or without acupuncture. Intestinal pathology was observed, and full transcriptome sequencing and bioinformatic analysis were performed. The results demonstrated that acupuncture treatment reduced the UC symptoms, disease activity index score, and histological colitis score and increased body weight, colon length, and the number of intestinal goblet cells. In addition, acupuncture can also decrease the expression of necrotic biomarker phosphorylates mixed lineage kinase domain-like pseudo kinase (p-MLKL). Full-length transcriptome analysis indicated that acupuncture reversed the expression of 987 of the 1918 upregulated differentially expressed genes (DEGs), and 632 of the 1351 downregulated DEGs induced by DSS. DEGs regulated by acupuncture were mainly involved in inflammatory responses and intestinal barrier pathways. The protein–protein interaction network analysis revealed that matrix metalloproteinases (MMPs) are important genes regulated by acupuncture. Gene set enrichment analysis revealed that extracellular matrix (ECM)–receptor interaction was an important target of acupuncture. In addition, alternative splicing analysis suggested that acupuncture improved signaling pathways related to intestinal permeability, the biological processes of xenobiotics, sulfur compounds, and that monocarboxylic acids are closely associated with MMPs. Overall, our transcriptome analysis results indicate that acupuncture improves intestinal barrier function in UC through negative regulation of MMPs expression.

Keywords: Acupuncture, full-length transcriptome, ulcerative colitis, differentially expressed genes, matrix metalloproteinases, alternative splicing

Experimental Biology and Medicine 2023; 248: 1229–1241. DOI: 10.1177/15353702231182205

Introduction

Ulcerative colitis (UC) is a chronic, complex immune-mediated inflammatory colon disease characterized by major lesions in the mucosa and submucosa of sigmoid colon and rectum,¹ persistent diffuse inflammation,² and injury of the intestinal mucosal barrier.³ Although the chronic and refractory nature of UC has prompted extensive research to develop effective therapies, current treatment modalities still suffer from significant drawbacks. As a complementary medicine approach, acupuncture has been extensively used to alleviate the symptoms

of UC.^{4,5} However, despite its protective effects, the specific mechanisms are still unclear.

Gene regulation is a basic process in disease occurrence and development.⁶ Transcriptome sequencing can capture the dynamic changes of the transcriptome in different tissues and during various pathophysiological states. By analyzing differences in gene transcription under the action of different factors, associations between genes with significantly different expression and biological functions can be established.⁷ Therefore, transcriptome analysis may serve as an effective method to characterize the transcriptional landscape of colon

tissues in order to elucidate both the pathogenesis of UC and the molecular mechanisms underlying acupuncture's beneficial effects. Thus, the purpose of this study was to analyze, through full-length transcriptomics of colon tissues from mice with dextran sodium sulfate (DSS)-induced UC, the major molecular targets and mechanisms mediating the beneficial effect of acupuncture treatment on UC. Besides, we carried out biological experiments and upstream alternative splicing (AS) analysis to validate the transcriptome sequencing results and to analyze the possible causes.

Materials and methods

Experimental animals

Twenty-four male C57BL/6J mice (SPF class, 26 ± 2 g) were provided from GemPharmatech (Nanjing, China). A special pathogen-free housing environment, normal diets, and 12 h of light/dark cycles were applied to the animals under ambient temperatures of $23 \pm 2^\circ\text{C}$. Protocols for animal experiments were approved by the Animal Experimental Ethics Committee of the Chengdu University of Traditional Chinese Medicine (approval no. 2019-04), in compliance with the National Institutes of Health guidelines for the care and use of laboratory animals.

Induction of UC in mice

We randomized mice into three groups ($n=8$ mice per group): control group, DSS group, and DSS + acupuncture (DSS + A) group. Mice in the DSS and DSS + A groups received 2.5% DSS (43 kDa, MP Biomedicals, Irvine, CA, USA) in drinking water for seven days as previously described,⁸ whereas the control group was given only normal drinking water. We evaluated body weight and fecal bleeding every day.

Acupuncture intervention

After five days of UC modeling, the mice in the DSS + A group were treated with acupuncture once a day for a total of five days. Then, animals were fixed on a custom mouse frame (CN210872183U) and needled at Zusanli acupoint (ST36, located ~3 mm below the capitulum fibulae). After insertion, the needles remained in position for 30 min, and acupuncture was performed every 5 min to strengthen the stimulation. The control group and the DSS group were also fixed following the same procedure for 30 min, without receiving any other intervention.

Disease activity index scoring

Body weight loss, feces status, and occult/bloody stools were recorded, and data combined to calculate disease activity index (DAI) score. Standards for evaluation are shown in Supplemental Table 1.

Histological scoring and periodic acid–Schiff staining

After five days of treatment, mice were euthanized, and colon sections were collected and processed for hematoxylin–eosin (HE) staining. A combined histological score was

calculated for inflammation extent and crypt damage. Each subscale score is presented in Supplemental Table 2. Paraffin sections were also stained with periodic acid–Schiff (PAS) to assess the presence of mucus droplets in goblet cells. Visual inspection was performed under light microscopy (Olympus, Tokyo, Japan).

Western blot

Protease and phosphatase inhibitors were added to RIPA lysis buffer to lyse proteins from colon tissue. The Bicinchoninic acid protein assay kit (Thermo, Rockford, IL, USA) was used to quantify protein concentrations. For western blotting, protein extracts (20 μg) from colon tissue were loaded onto FuturePAGE™ gel (ACE, ET15420GEL, Nanjing, China) and transferred to polyvinylidene fluoride (PVDF) (Servicebio, Wuhan, China) membranes. The membranes were then blocked with 5% non-fat dry milk in Tris-buffered saline/Tween 20 (TBST, Servicebio) and incubated with primary antibodies (anti-MLKL, anti-p-MLKL, anti-MMP9, anti-GAPDH) overnight at 4°C . The secondary antibody was then incubated for an additional 2 h. The following primary antibodies were used: anti-MLKL (ABclonal (Woburn, MA, USA), A5579, 1:1000), anti-p-MLKL (ABclonal, AP0949, 1:1000), anti-MMP9 (Proteintech (Rosemont, IL, USA), 10375-2-AP, 1:1000), anti-GAPDH (Proteintech, 60004-1-Ig, 1:5000).

RNA extraction, library construction, and full-length transcriptome sequencing

Colon tissues from mice in each experimental group (three mice per group) were digested for the extraction of total RNA, and a complementary DNA (cDNA) library was generated following a protocol provided by Oxford Nanopore Technology (ONT, Oxford, UK). Briefly, the SuperScript IV first-chain synthesis system was used to perform reverse transcription, and the cDNA was amplified by 14 polymerase chain reaction (PCR) cycles using LongAmp Taq DNA polymerase (New England Biolabs, NEB, Ipswich, MA, USA). Following FFPE DNA repair and terminal repair steps (NEB), the PCR product was ligated with T4 DNA ligase (NEB). DNA was purified using Agencourt XP beads according to the ONT protocol. Sequencing was performed by Biomarker Technologies Corp (Beijing, China) using a PromethION sequencing platform (ONT) on flu-Min 109 stream cells. For quality control of the library, the Nanodrop2000 nucleic acid analyzer was used to test the quality of the RNA sample and quality control was performed using LabChip GX. Qualified samples met all of the following conditions: concentration ≥ 40 ng/ μL , volume ≥ 10 μL , OD260/280 of 1.7–2.5 and OD260/230 of 0.5–2.5, 260 nm absorption peak display normal, and RNA integrity number (RIN) value ≥ 8 .

Analysis of full-length transcriptome data

As a first step, the original reads were filtered to select those with a minimum mean quality score of 7 and a minimum length of 500 bases. Then, we mapped ribosomal RNA to the rRNA database and discarded it. After looking for primers on both ends of each read, FLNC (full-length, non-chimeric) transcripts were identified and mapped to the

reference genome by MIMimap2. Consensus subtypes were obtained by polishing within each cluster by Pinfish. Using GFFCompare, transcripts were validated against reference transcript annotations. The AStalavista tool was used to identify AS events, including exon skipping (ES), alternative 3' splice sites (A3SS), mutually exclusive exons (ME), alternative 5' splice sites (A5SS), and intron retention (IR). And differentially expressed genes (DEGs) between experimental groups were identified using the DESeq2 R software package (3.6.3) and defined as those with an absolute P value < 0.01 and $|\log_2(\text{fold change})| > 1.5$.⁹ DEGs were subjected to Gene Ontology (GO) functional enrichment and Kyoto Encyclopedia of Genes and Genomes (KEGG) pathway enrichment analyses using DAVID (<https://david.ncifcrf.gov/>) and Metascape (<http://metascape.org/>).^{10,11}

Quantitative real-time polymerase chain reaction

Total RNA was isolated from colon tissues using a MolPure® TRIeasy™ Plus Total RNA Kit (Yeasen, Shanghai, China) and cDNA prepared using a Hifair® III 1st Strand cDNA Synthesis Super Mix (Yeasen), according to the manufacturer's instructions. The Hieff® qPCR SYBR® Green Master Mix (Yeasen) and a Bio-Rad CFX Maestro real-time PCR system (Bio-Rad, Hercules, CA, USA) were used for quantitative polymerase chain reaction (qPCR) detection. The $2^{-\Delta\Delta Ct}$ method was used to calculate relative mRNA expression of target genes, using β -actin expression levels as endogenous control. Primer sequences are listed in Supplemental Table 3.

Immunohistochemistry

After dewaxing, tissue sections were placed in citric acid buffer (pH 6.0) and microwaved for 20 min. Endogenous peroxidase activity was blocked by applying a catalase inhibitor for 10 min, followed by blocking of unspecific antibody reactions with 5% fetal bovine serum for 2 h. Primary antibodies raised against Claudin-1 (Proteintech, 13050-1-AP, 1:200), ZO-1 (Proteintech, 21773-1-AP, 1:100), and Occludin (Proteintech, 66378-1-IG, 1:100) were applied at 4°C overnight. After incubation with suitable horseradish peroxidase (HRP)-labeled secondary antibodies for 2 h, samples were incubated in 3,3'-diaminobenzidine (DAB, Servicebio) for 1 min and counterstained with hematoxylin before mounting. Sections were then scanned with a digital whole-slide HS60 instrument (Sunny, Shanghai, China).

Statistical analysis

Statistical analysis was performed using SPSS 22.0 software (IBM, Chicago, IL, USA). Values are expressed as mean value \pm SEM. Unpaired Student's t -test and one-way analysis of variance (ANOVA) were used to compare means between two groups. $P < 0.05$ was considered statistically significant.

Results

Acupuncture attenuates UC severity in DSS model mice

The effects of acupuncture on DSS-induced UC mice were first evaluated by measuring body weight, computing DAI,

and examining histopathological characteristics. Compared to the DSS group, DSS + A mice had higher body weight (Figure 1(A)), lower DAI scores (Figure 1(B)), and longer colon length (Figure 1(C) and (D)). Colon tissue was stained with HE for the assessment of colitis severity, while PAS staining was used for detection of intestinal goblet cells. Compared with the control group, mice in the DSS group showed overt necrosis and edema of the colonic mucosa, disappearance of crypt structures, and diffuse infiltration of inflammatory cells. In contrast, mice in the DSS + A group showed preserved colon morphology and reduced inflammation and leukocyte infiltration (Figure 1(E) and (F)). In turn, PAS staining showed that DSS administration led to a significant reduction in mucus production and the number of goblet cells. In particular, acupuncture effectively reversed this effect (Figure 1(E) and (G)). We then detected necrotic biomarker phosphorylates mixed lineage kinase domain-like pseudo kinase (p-MLKL) in the colonic tissue by western blot (WB). Compared with the control group, mice in the DSS group showed significantly increased p-MLKL expression, which was effectively reversed by acupuncture treatment (Figure 1(H)–(J)). These findings suggest that acupuncture improves the necrosis of colon tissue.

Acupuncture alters inflammatory gene expression to improve intestinal barrier function in UC

To identify mechanisms by which acupuncture treatment attenuates UC severity, ONT's nanopore technology was used to analyze transcriptome profiles in the different groups. The volcano plot of RNA-seq results revealed that compared to the control group, there were 3269 DEGs in the DSS group, including 1918 upregulated and 1351 downregulated genes (Figure 2(A)). We also found 2028 DEGs between the DSS + A and the DSS group. Among these, 859 were upregulated and 1169 were downregulated (Figure 2(B)). Analysis of gene expression patterns based on ONT data is depicted in a heatmap (Figure 2(C)). Then, we assessed DEGs overlap using the Venn diagram analysis. We found that acupuncture reversed the expression of 987 of the 1918 upregulated DEGs and of 632 of the 1351 downregulated DEGs detected in the DSS group (Figure 2(D)).

We next performed functional enrichment analysis of DEGs in the GO and KEGG databases. In the GO database, genes were annotated based on three different ontologies: BP, CC, and MF, we extracted from each one the top five enriched terms (Figure 2(E)). In the BP category, DEGs were mainly enriched in positive regulation of cytokine production, leukocyte migration, and regulation of inflammatory response (Supplemental Figure 1(A)). For CC category, the most enriched terms included integral component of membrane, extracellular space, and extracellular matrix (Supplemental Figure 1(B)). For MF category, DEGs enrichment was mainly detected in cytokine activity, receptor ligand activity, and cytokine receptor binding (Supplemental Figure 1(C)). KEGG pathway analysis showed that cytokine–cytokine receptor interaction, PI3K–Akt signaling pathway, mitogen-activated protein kinase (MAPK) signaling pathway, nucleotide oligomerization domain (NOD)-like receptor signaling pathway, and tumor necrosis factor (TNF) signaling pathway

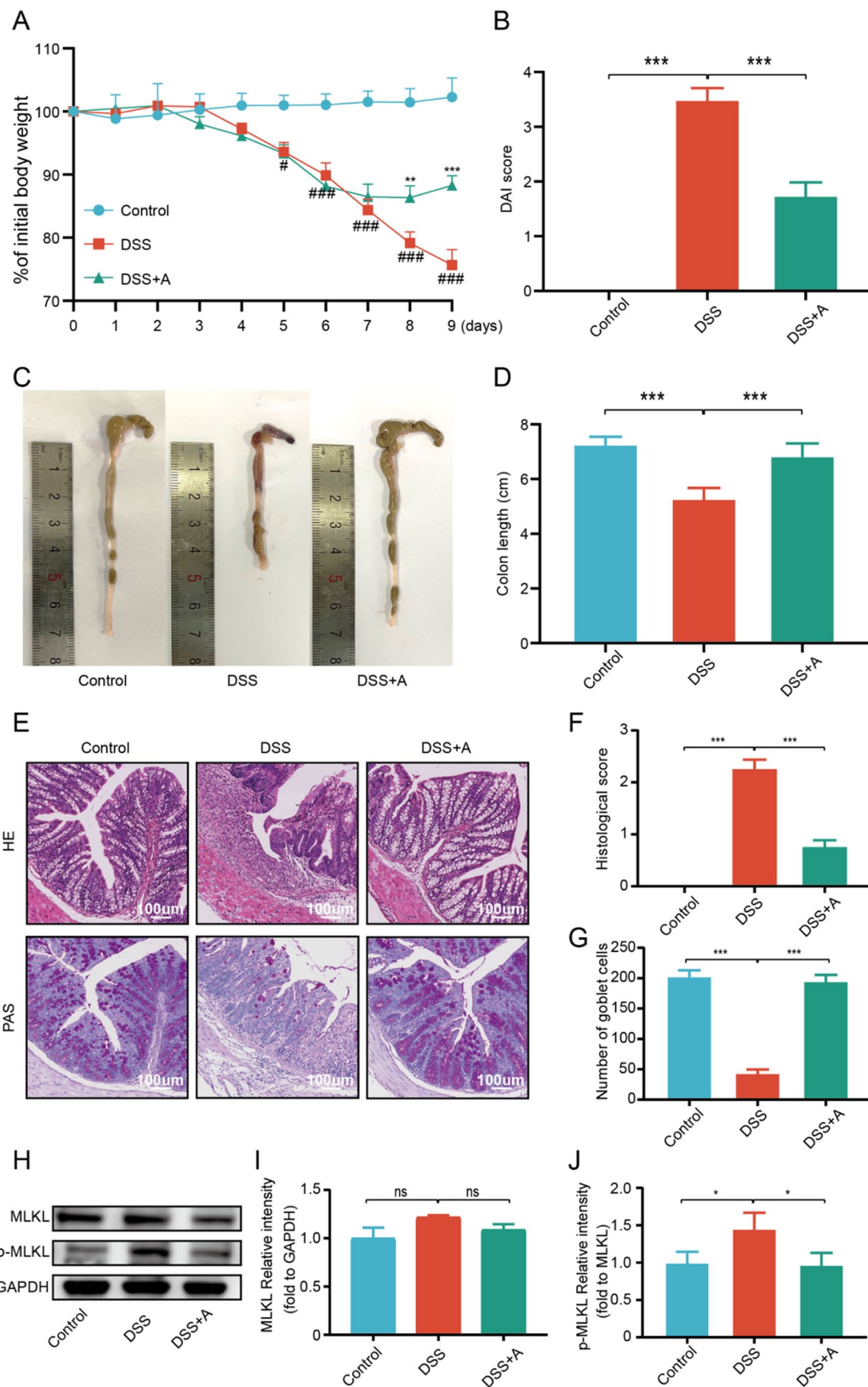


Figure 1. Acupuncture relieves DSS-induced UC in mice. (A) Body weight changes ($n=8$) showing that acupuncture improved body weight loss in UC model mice. (B) DAI score ($n=8$). Acupuncture improves DAI score in DSS mice. (C) Representative images of excised colons. The colon was obviously congested and shortened after DSS modeling and alleviated after acupuncture. (D) Colon length measurements ($n=6$). Acupuncture significantly increased colon length in DSS mice. (E) Representative images of HE and PAS staining in colon tissues (magnification=200 \times , scale 100 μ m). (F) Histological score ($n=6$). DSS group showed overt necrosis and edema of the colonic mucosa, disappearance of crypt structures, and diffuse infiltration of inflammatory cells and alleviated obviously in acupuncture group. (G) Number of goblet cells ($n=6$). DSS administration led to a significant reduction in mucus production and goblet cells numbers, acupuncture effectively reversed this effect. (H) Western blotting of MLKL and p-MLKL expression in colon tissues. (I) The relative intensities of MLKL were normalized against GAPDH ($n=4$). There was no significant difference in MLKL expression among all groups. (J) The relative intensities of p-MLKL normalized against MLKL ($n=4$). Compared with control group and DSS group, p-MLKL expression was significantly increased. After acupuncture intervention, p-MLKL decreased significantly. Data are shown as mean value \pm SEM. ** $P < 0.01$; *** $P < 0.001$.

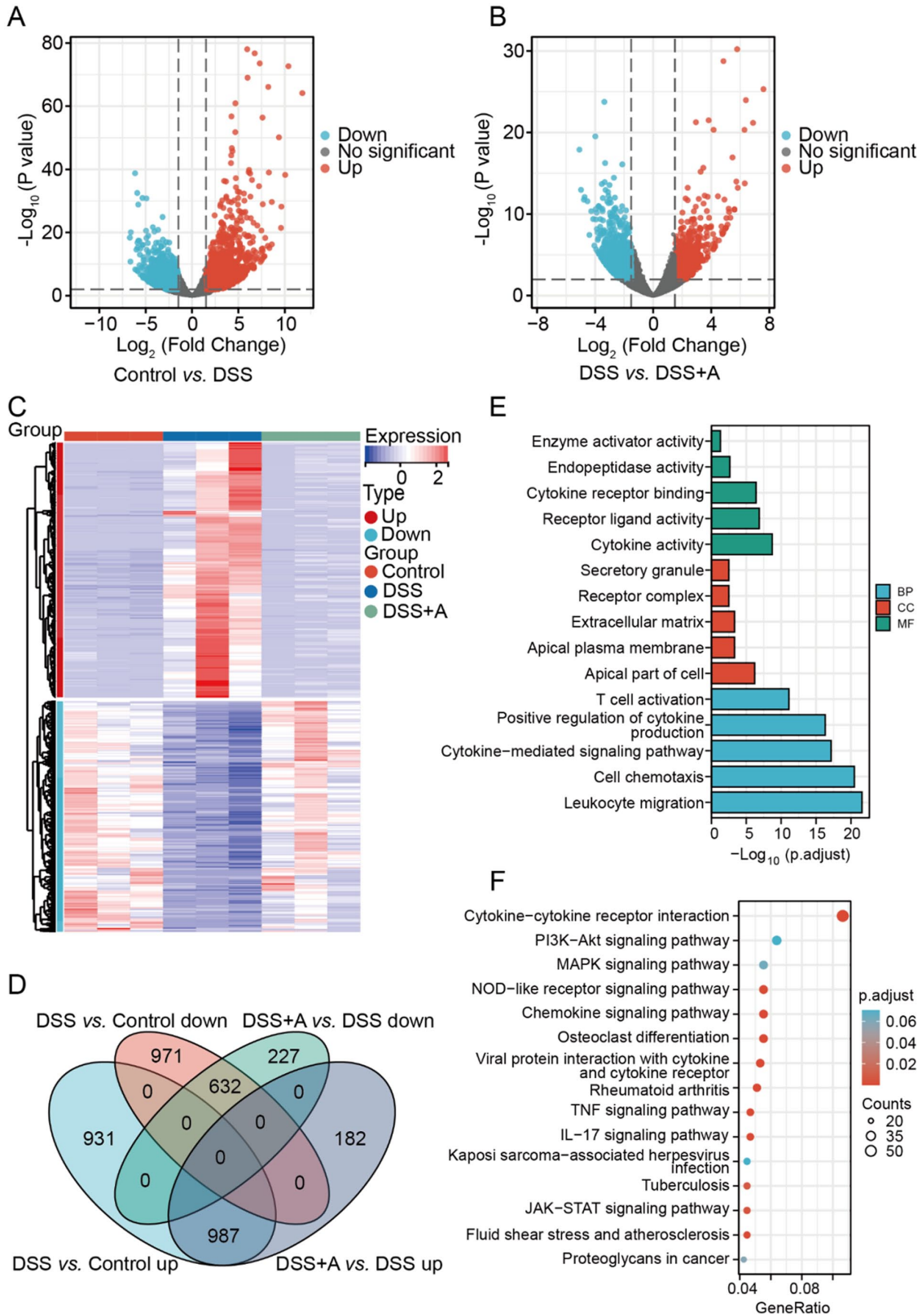


Figure 2. Full-length transcriptome analysis of differential gene expression. (A) Volcano plot for DEGs between the DSS and the control group ($\text{log}_2\text{FCI} > 1.5$, $P < 0.01$). Red dots represent the upregulated genes, blue dots represent the downregulated genes, and black dots represent the genes with no significant changes. (B) Volcano plot for DEGs between the DSS + A and the DSS group ($\text{log}_2\text{FCI} > 1.5$, $P < 0.01$). Red dots represent the upregulated genes, blue dots represent the downregulated genes, and black dots represent the genes with no significant changes. (C) Heatmaps of upregulated and downregulated genes in the control, DSS, and DSS + A groups. The DEGs were classified into different cluster groups based on gene expression similarity. The red to blue gradients represented the up to down of gene expressions. (D) Venn Diagram of DEGs. Acupuncture reversed the expression of 987 of the 1918 upregulated DEGs and of 632 of the 1351 downregulated DEGs detected in the DSS group. (E) GO terms enriched in DEGs. BP terms are shown in blue, CC terms are shown in red, and MF terms are shown in green. (F) KEGG pathways enriched in DEGs. The bubble size of the circle represents the counts value. The smaller the P value, the redder the color, and the larger the P value, the bluer the color.

ranked first among the top 15 pathways enriched by the acupuncture-regulated DEGs (Figure 2(F)). These findings suggest that acupuncture treatment ameliorates UC severity by regulating intestinal inflammation and barrier function.

Acupuncture attenuates UC by inhibiting matrix metalloproteinases

The STRING database (<http://string-db.org>) was used to construct a protein–protein interaction (PPI) network based on the identified DEGs.¹² We uploaded 1619 DEGs (Supplemental Figure 2) and extracted the top 50 hub genes using the cytoHubba plugin of Cytoscape (Figure 3(A)).^{13,14} We found that *Mmp9* is the node of the core network, while many other matrix metalloproteinase (MMP)-encoding genes also ranked among the top 50 hub genes. After extracting the *Mmp9*-centered module from the whole PPI network (Figure 3(B)), we selected gelatinases (*Mmp2*, *Mmp9*), stromelysins (*Mmp3*, *Mmp10*), collagenases (*Mmp8*, *Mmp13*), and macrophage elastase (*Mmp12*) for quantitative real-time polymerase chain reaction (qRT-PCR) validation (Figure 3(C) and (D)). The results of qRT-PCR confirmed that the expression trend of different experimental groups was similar to the results from RNA-seq (Figure 3(C) and (D)). Then, we verified the protein level of the core network's node gene *Mmp9* with WB. As shown in Figure 3(E), DSS group were significantly higher than those of the control group. In contrast, acupuncture treatment significantly reduced the upregulation of MMP9 induced by DSS. These results strongly suggested that acupuncture protects against UC by preventing the upregulation of MMPs.

Since MMPs are important mediators of intestinal barrier disruption during inflammatory injury,^{15,16} we evaluated whether the downregulation of MMPs mediated by acupuncture is related to the salvage expression of intestinal tight junction proteins such as Claudin-1, ZO-1, and Occludin. Immunohistochemistry (IHC) analysis revealed that compared with the control group, the expression levels of these three proteins in the DSS group decreased. On the contrary, Claudin-1, ZO-1, and Occludin expression was markedly preserved in the DSS + A group (Figure 3(F)). These results suggest that there may be a plausible correlation between the inhibition of MMPs expression and the protection of intestinal barrier function after acupuncture treatment in UC mice.

Analysis of acupuncture-regulated pathways via gene set enrichment analysis

Next, gene set enrichment analysis (GSEA) (www.broadinstitute.org/gsea/index.jsp) was applied to identify the main molecular functions regulated by acupuncture treatment in DSS-induced mice.¹⁷ In the comparison between the control group and the DSS group, we listed the top five upregulated and downregulated pathways retrieved from the KEGG database (Figure 4(A)). Compared with the control group, the main pathways of DSS-upregulated were cytokine–cytokine receptor interaction and extracellular matrix (ECM)–receptor interaction (Figure 4(B)). The top five upregulated and downregulated pathways between

the DSS and the DSS + A group are shown in Figure 4(C). Interestingly, compared with the DSS group, the DSS + A group detected significant downregulation of the cytokine–cytokine–receptor interaction and ECM–receptor interaction pathways, indicating that the effect mediated by DSS was reversed (Figure 4(D)). Since intestinal barrier function is strongly affected by the interaction between cytokine–receptor and ECM–receptor that modulate inflammatory responses and MMPs activity, these findings further suggest that net of anti-inflammatory and ECM-protective mechanisms mediates the protective effect of acupuncture on UC.

Identification of AS events in UC

AS plays a significant role maintaining protein diversity in cells and tissues.¹⁸ Previous studies indicated that AS events contribute to differential gene expression related to the occurrence and development of UC.¹⁹ The analysis of RNA-seq data using the AStalavista platform to support the notion of AS is a common phenomenon in UC. Splicing events are categorized into five main types: ES, A3SS, ME, IR, and A5SS (Figure 5(A)). In colon samples from the control group, 2205 ES-type AS events involving 791 genes, 778 A3SS-type AS events involving 388 genes, 681 A5SS-type AS events involving 380 genes, 670 IR-type AS events involving 280 genes, and 199 ME-type AS events involving 62 genes were detected (Figure 5(B)). The AS type distribution of the control group is shown in Figure 5(C). In the DSS group, 4624 ES-type AS events involving 1437 genes, 1060 A3SS-type AS events involving 443 genes, 861 A5SS-type AS events involving 382 genes, 871 IR-type AS events involving 340 genes, and 241 ME-type AS events involving 90 genes were identified (Figure 5(D)). The AS type distribution of DSS group is shown in Figure 5(E). In the DSS + A group, 3542 ES-type AS events involving 1276 genes, 1008 A3SS-type AS events involving 502 genes, 792 A5SS-type AS events involving 426 genes, 778 IR-type AS events involving 362 genes, and 244 ME-type AS events involving 91 genes were recorded (Figure 5(F)). The AS type distribution of DSS + A group is presented in Figure 5(G). These results revealed that ES was the predominant AS event in all three groups.

Acupuncture regulates differential AS events in UC

The Venn intersection analysis revealed the presence of AS events in a total of 858 genes common to the three experimental groups (Figure 6(A)). Compared to the control group, there were 20 upregulated and 68 downregulated AS-related genes in the DSS group (Figure 6(B)). Compared to the DSS group, there were 46 upregulated and 7 downregulated AS-related genes in the DSS + A group (Figure 6(B)). The Venn diagram analysis of the above genes showed that acupuncture treatment affected AS in a total of 40 differential genes regulated by UC (Figure 6(C)). Interestingly, these genes were identified as colorectal specific by Metascape (Figure 6(D)). In turn, GO analysis indicated these genes were highly enriched in xenobiotic metabolic process, sulfur compound metabolic process, and monocarboxylic acid metabolic process (Figure 6(E)).

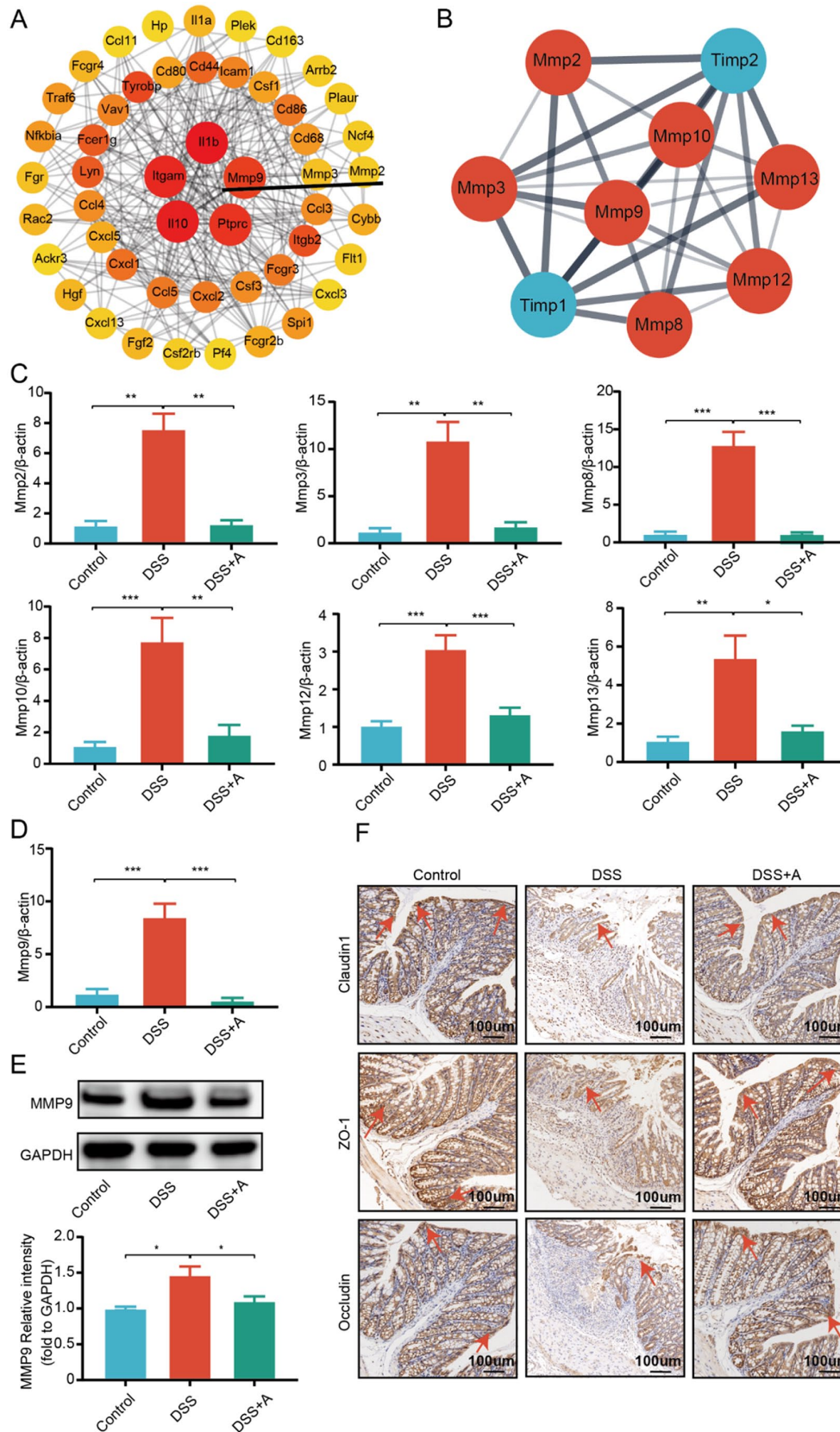


Figure 3. Acupuncture inhibits the expression colonic MMPs and maintains intestinal barrier function in the DSS mouse model of UC. (A) Top 50 hub DEGs identified by cytoHubba. The red-yellow color gradient reflects (from high to low) each node's connection degree. (B) Subnetwork of MMP-related genes identified in STRING. Red indicates MMPs family members, the thicker the connection line, the higher the interaction strength. (C) Relative expression of MMPs mRNAs (including *Mmp2*, *Mmp3*, *Mmp10*, *Mmp12*, *Mmp13*, *n=6*). After DSS modeling, the expression of MMPs was significantly increased, and acupuncture could significantly inhibit the expression. (D) Relative expression of *Mmp9* mRNAs. (E) Western blotting of MMP9 expressions in colon tissues (*n=4*). DSS group were significantly higher than those of the control group. In contrast, acupuncture treatment significantly reduced DSS-induced upregulation of MMP9. (F) Representative images of Claudin-1, ZO-1, and Occludin IHC in colonic tissue (magnification=200×, scale 100μm). Red arrows indicate immunoreactivity. Data are shown as mean value ± SEM. **P* < 0.05; ***P* < 0.01; ****P* < 0.001.

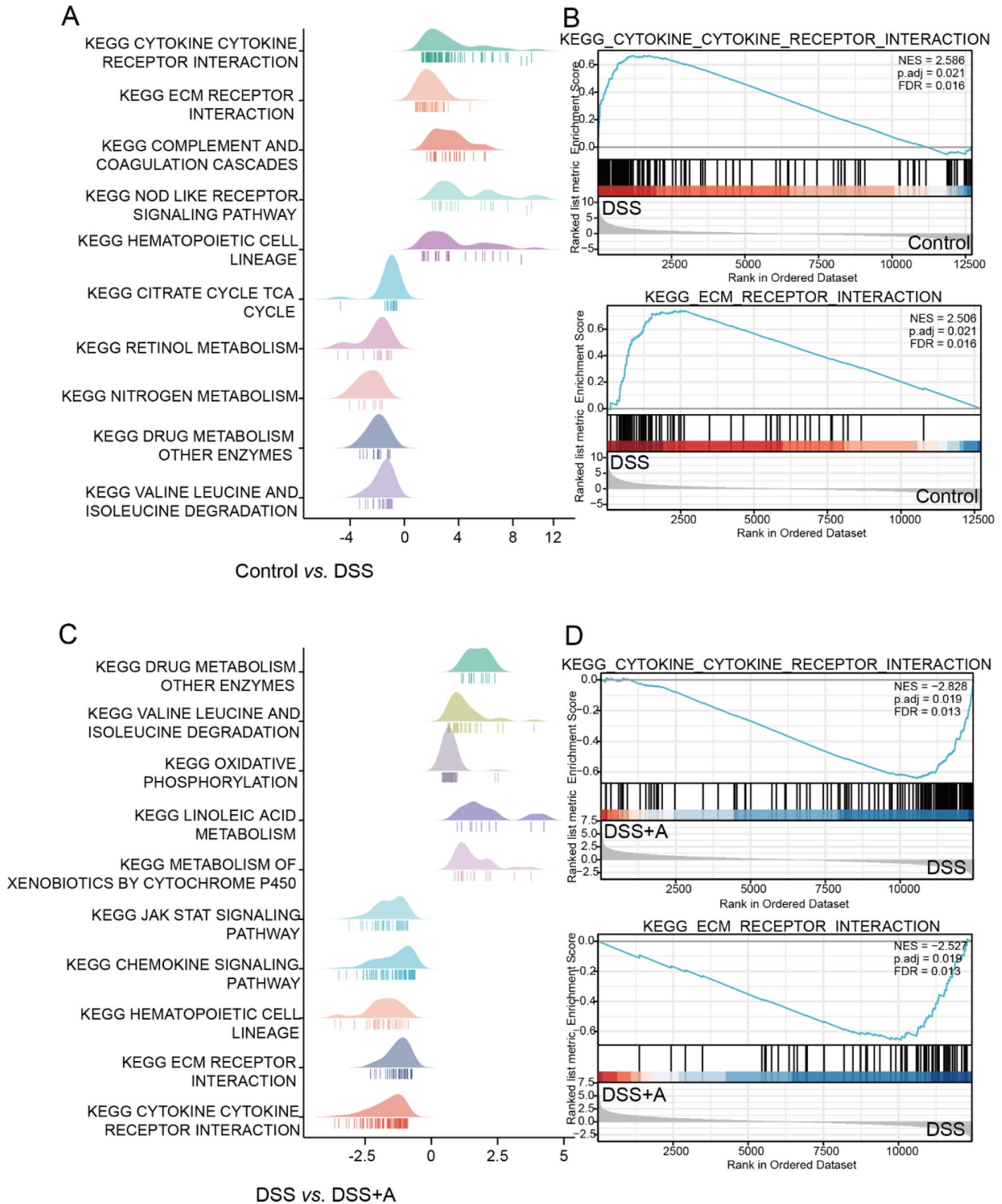


Figure 4. GSEA of acupuncture-regulated genes in UC. GSEA analysis showing cytokine–cytokine receptor interaction and ECM–receptor interaction were the top two pathways influenced by acupuncture in mice with DSS-induced UC. (A) Top five positively and negatively enriched pathways in the DSS group versus the control group. (B) Positively enriched pathways in the DSS group versus the control group. Compared with the control group, cytokine–cytokine receptor interaction and ECM–receptor interaction were main DSS-upregulated pathways. (C) Top five positively and negatively enriched pathways in the DSS + A group versus the DSS group. (D) Negatively enriched pathways in the DSS + A group versus the DSS group. Compared with the DSS group, cytokine–cytokine receptor interaction and ECM–receptor interaction were the main acupuncture-downregulated pathways.

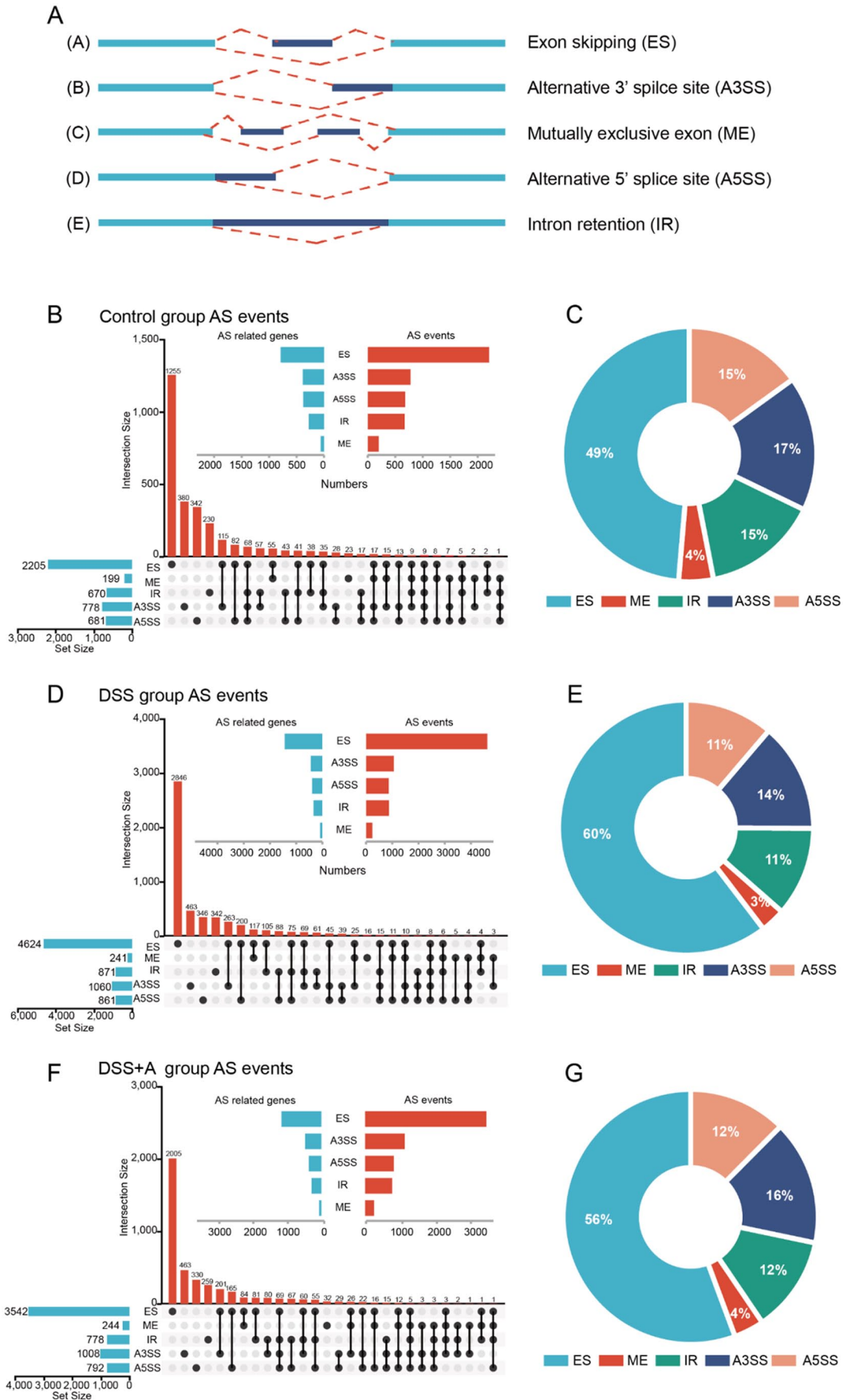


Figure 5. AS events statistics showing the frequency and distribution of the different AS events in the DSS + A group were more resemblant to those observed in the control, rather than in the DSS group. (A) AS events patterns. (B) Graph of interactions between genes and AS events for the control group. (C) AS events distribution in the control group. (D) Graph of interactions between genes and AS events for the DSS group. (E) AS events distribution in the DSS group. (F) Graph of interactions between genes and AS events for the DSS + A group. (G) AS events distribution in the DSS + A group.

Discussion

High-throughput sequencing provides a new and reliable method to comprehensively evaluate and screen the targets of different interventions. Previous studies on UC used second-generation sequencing (SGS).^{20–22} However, the short read RNA-seq data provided by SGS cannot identify or quantify the transcriptional isoforms produced by individual genes.²³ Compared to SGS, the third-generation full-length transcriptome sequencing technology used in this study overcomes the technical problems such as short splicing and incomplete transcript structure. This allows more complete, comprehensive, and accurate acquisition of sequencing data,²⁴ facilitating the analysis of both the complexity of the transcriptome in UC and the transcriptional changes induced by acupuncture treatment.

Many studies have confirmed the therapeutic effects of acupuncture on UC from different aspects such as intestinal flora regulation,²⁵ immunity balance,^{26,27} and protection of the intestinal barrier;²⁸ the key targeted effects are still unclear. Our results revealed that the DEGs identified by the third-generation full-length transcriptome sequencing technology are mainly enriched in leukocyte migration, cell chemotaxis, cytokine-mediated signaling pathway, positive regulation of cytokine production, and T-cell activation. The main KEGG pathways are enriched in the acupuncture-regulated DEGs including cytokine–cytokine receptor interaction, the PI3K–Akt, MAPK, and NOD-like receptor signaling pathways. Since most of these pathways have been reported to be associated with inflammation and the intestinal barrier,^{29–33} we speculate that acupuncture intervention targets mainly focus on inflammation and mucosal protection.

The following analysis of the core network node shows that MMPs are the most important targets in the DSS-induced mice treated by acupuncture. In addition, the qRT-PCR assay results of the expression of gelatinases (*Mmp2*, *Mmp9*), stromal lysins (*Mmp3*, *Mmp10*), collagenases (*Mmp8*, *Mmp13*), and macrophage elastase (*Mmp12*) are consistent with the RNA-seq data, which confirms the reliability of the above transcriptomics results. Next, based on the GSEA and AS analysis results, the “cytokine–cytokine receptor interaction” and the ECM–receptor interaction were the top two pathways influenced by acupuncture in mice with DSS-induced UC. The 40 identified genes for AS were associated with the metabolism of xenobiotics, sulfur compounds, and monocarboxylic acids. MJ Tsai and colleagues^{34–38} reported that the metabolic pathways of xenobiotics, sulfur compounds, and monocarboxylic acids are closely related to intestinal microorganisms and intestinal barrier function. What’s more, the National Institutes of Health (NIH) Human Microbiome Project (HMP) metagenomes, analyzed by Rajakovich and Balskus, showed that the metalloenzyme superfamily SAM was the most prevalent in the human gut microbiota,³⁹ indicating that MMP-related biological processes are essential for the health of the gastrointestinal tract.

MMPs are a class of neutral proteases that can degrade all components of ECM,¹⁶ leading to infiltration of immune cells and the breakdown of the intestinal barrier.^{40,41} The relationship between MMPs and colitis has long been discovered, and they are an important class of enzymes for all fields of life. In particular, recent studies have shown that MMPs can

be used as markers of intestinal ulcers or inflammatory bowel diseases.⁴² This role of MMPs may be related to their key role and universality in the interaction between intestinal flora and host.³⁹ Studies have shown that MMPs not only mediate the sulfation and fucosylation of glycans and promote the colonization of intestinal flora in the mucosa,^{43,44} but also form colonization resistance to intestinal pathogenic microorganisms by participating in the synthesis of bacteriocin.⁴⁵ Besides, MMPs participate in the synthesis of vitamin, trimethylamine, *p*-cresol, hydrogen sulfide and other metabolites, and in the transformation of exogenous active substances from drugs or plants, so as to promote host health or induce disease.^{46–50} Therefore, to some extent, the health status of the gut can be predicted by assessing the abundance and distribution of the MMP family in the human gut microbiota.⁵¹

How MMPs works in the gut? It has been suggested that metallocofactors can play a significant role by enabling unique molecular rearrangements and transformations. In the hypoxic environment of the human colon, anaerobic bacteria utilize metalloenzymes to perform many metabolic functions that allow gut microbes to obtain nutrients or energy from alternative substrates or to produce molecules that have important effects on the host.³⁹ Moreover, IHC staining results of Claudin-1, ZO-1, and Occludin in intestinal barrier also support the possibility that acupuncture protects intestinal barrier function, intestinal inflammation, and the metabolic interaction of the host-intestinal microbiota by inhibiting MMP-related proteins.

In conclusion, through full-length transcriptome technology, we identified the MMP family as the key targets of acupuncture treatment in UC. This therapeutic effect of acupuncture has also been analyzed as it may be closely related to intestinal mucosal protection, intestinal inflammation, and metabolic interaction of host-intestinal microbiota by MMPs.

AUTHORS' CONTRIBUTIONS

All authors participated in the design, interpretation of the studies, and review of the manuscript. R-BZ, L-CD, QH, and YS participated in the collection and assembly of data. R-BZ, L-CD, and H-YL performed the analysis of the data; R-BZ, QH, and YS. conducted the experiments; R-BZ, Q-FW, and S-GY wrote the manuscript.

ACKNOWLEDGEMENTS

The Chengdu University of Traditional Chinese Medicine Acupuncture and Tuina School technical team deserves our gratitude.

DECLARATION OF CONFLICTING INTERESTS

The author(s) declared no potential conflicts of interest with respect to the research, authorship, and/or publication of this article.

FUNDING

The author(s) disclosed receipt of the following financial support for the research, authorship, and/or publication of this article: This study was supported by the National Key R&D Program of China (no. 2019YFC1709001), the National Natural Science Foundation of China (nos 82174512, 81873383), the Innovation Team and Talents Cultivation Program of

National Administration of Traditional Chinese Medicine (no. ZYYCXTD-D-202003), and the Fund of Science and Technology Department of Sichuan Province, China (nos 2021ZYD0081, 2022ZDZX0033).

ORCID ID

Qiao-Feng Wu  <https://orcid.org/0000-0002-8870-6707>

SUPPLEMENTAL MATERIAL

Supplemental material for this article is available online.

REFERENCES

- Ungaro R, Mehandru S, Allen PB, Peyrin-Biroulet L, Colombel JF. Ulcerative colitis. *Lancet* 2017;**389**:1756–70
- Peters LA, Perrigoue J, Mortha A, Iuga A, Song WM, Neiman EM, Llewellyn SR, Di Narzo A, Kidd BA, Telesco SE, Zhao Y, Stojmirovic A, Sendeki J, Shameer K, Miotto R, Losic B, Shah H, Lee E, Wang M, Faith JJ, Kasarskis A, Brodmerkel C, Curran M, Das A, Friedman JR, Fukui Y, Humphrey MB, Iritani BM, Sibinga N, Tarrant TK, Argmann C, Hao K, Roussos P, Zhu J, Zhang B, Dobrin R, Mayer LF, Schadt EE. A functional genomics predictive network model identifies regulators of inflammatory bowel disease. *Nat Genet* 2017;**49**:1437–49
- Dotti I, Mora-Buch R, Ferrer-Picón E, Planell N, Jung P, Masamunt MC, Leal RF, Martín de Carpi J, Llach J, Ordás I, Batlle E, Panés J, Salas A. Alterations in the epithelial stem cell compartment could contribute to permanent changes in the mucosa of patients with ulcerative colitis. *Gut* 2017;**66**:2069–79
- Langhorst J, Wulfert H, Lauche R, Klose P, Cramer H, Dobos GJ, Korzenik J. Systematic review of complementary and alternative medicine treatments in inflammatory bowel diseases. *J Crohns Colitis* 2015;**9**:86–106
- Wang X, Zhao NQ, Sun YX, Bai X, Si JT, Liu JP, Liu ZL. Acupuncture for ulcerative colitis: a systematic review and meta-analysis of randomized clinical trials. *BMC Complement Med Ther* 2020;**20**:309
- Lee TI, Young RA. Transcriptional regulation and its misregulation in disease. *Cell* 2013;**152**:1237–51
- Wang Z, Gerstein M, Snyder M. RNA-Seq: a revolutionary tool for transcriptomics. *Nat Rev Genet* 2009;**10**:57–63
- Wang S, Lin Y, Li F, Qin Z, Zhou Z, Gao L, Yang Z, Wang Z, Wu B. An NF- κ B-driven lncRNA orchestrates colitis and circadian clock. *Sci Adv* 2020;**6**:eabb5202
- Love MI, Huber W, Anders S. Moderated estimation of fold change and dispersion for RNA-seq data with DESeq2. *Genome Biol* 2014;**15**:550
- Yu G, Wang LG, Han Y, He QY. clusterProfiler: an R package for comparing biological themes among gene clusters. *OMICS* 2012;**16**:284–7
- Zhou Y, Zhou B, Pache L, Chang M, Khodabakhshi AH, Tanaseichuk O, Benner C, Chanda SK. Metascape provides a biologist-oriented resource for the analysis of systems-level datasets. *Nat Commun* 2019;**10**:1523
- Szklarczyk D, Gable AL, Nastou KC, Lyon D, Kirsch R, Pyysalo S, Doncheva NT, Legeay M, Fang T, Bork P, Jensen LJ, von Mering C. Correction to “The STRING database in 2021: customizable protein-protein networks, and functional characterization of user-uploaded gene/measurement sets.” *Nucleic Acids Res* 2021;**49**:10800
- Chin CH, Chen SH, Wu HH, Ho CW, Ko MT, Lin CY. cytoHubba: identifying hub objects and sub-networks from complex interactome. *BMC Syst Biol* 2014;**8**:S11
- Otasek D, Morris JH, Boucas J, Pico AR, Demchak B. Cytoscape Automation: empowering workflow-based network analysis. *Genome Biol* 2019;**20**:185
- Lin JC, Wu JQ, Wang F, Tang FY, Sun J, Xu B, Jiang M, Chu Y, Chen D, Li X, Su S, Zhang Y, Wu N, Yang S, Wu K, Liang J. QingBai decoction regulates intestinal permeability of dextran sulphate sodium-induced colitis through the modulation of notch and NF- κ B signalling. *Cell Prolif* 2019;**52**:e12547
- Maronek M, Marafini I, Gardlik R, Link R, Troncone E, Monteleone G. Metalloproteinases in inflammatory bowel diseases. *J Inflamm Res* 2021;**14**:1029–41
- Subramanian A, Tamayo P, Mootha VK, Mukherjee S, Ebert BL, Gillette MA, Paulovich A, Pomeroy SL, Golub TR, Lander ES, Mesirov JP. Gene set enrichment analysis: a knowledge-based approach for interpreting genome-wide expression profiles. *Proc Natl Acad Sci U S A* 2005;**102**:15545–50
- Ule J, Blencowe BJ. Alternative splicing regulatory networks: functions, mechanisms, and evolution. *Mol Cell* 2019;**76**:329–45
- Low END, Mokhtar NM, Wong Z, Raja Ali RA. Colonic mucosal transcriptomic changes in patients with long-duration ulcerative colitis revealed colitis-associated cancer pathways. *J Crohns Colitis* 2019;**13**:755–63
- Shi YJ, Hu SJ, Zhao QQ, Liu XS, Liu C, Wang H. Toll-like receptor 4 (TLR4) deficiency aggravates dextran sulfate sodium (DSS)-induced intestinal injury by down-regulating IL6, CCL2 and CSF3. *Ann Transl Med* 2019;**7**:713
- Fenton CG, Taman H, Florholmen J, Sorbye SW, Paulssen RH. Transcriptional signatures that define ulcerative colitis in remission. *Inflamm Bowel Dis* 2021;**27**:94–105
- Lu H, Lin J, Xu C, Sun M, Zuo K, Zhang X, Li M, Huang H, Li Z, Wu W, Feng B, Liu Z. Cyclosporine modulates neutrophil functions via the SIRT6-HIF-1 α -glycolysis axis to alleviate severe ulcerative colitis. *Clin Transl Med* 2021;**11**:e334
- Shaaban S, Cowley LA, McAteer SP, Jenkins C, Dallman TJ, Bono JL, Gally DL. Evolution of a zoonotic pathogen: investigating prophage diversity in enterohaemorrhagic *Escherichia coli* O157 by long-read sequencing. *Microb Genom* 2016;**2**:e000096
- Byrne A, Cole C, Volden R, Vollmers C. Realizing the potential of full-length transcriptome sequencing. *Philos Trans R Soc Lond B Biol Sci* 2019;**374**:20190097
- Liu GH, Liu HM, Chen YS, Lee TY. Effect of electroacupuncture in mice with dextran sulfate sodium-induced colitis and the influence of gut microbiota. *Evid Based Complement Alternat Med* 2020;**2020**:2087903
- Tian L, Huang YX, Tian M, Gao W, Chang Q. Downregulation of electroacupuncture at ST36 on TNF- α in rats with ulcerative colitis. *World J Gastroenterol* 2003;**9**:1028–33
- Jin H, Guo J, Liu J, Lyu B, Foreman RD, Shi Z, Yin J, Chen JDZ. Auto-nomically mediated anti-inflammatory effects of electrical stimulation at acupoints in a rodent model of colonic inflammation. *Neurogastroenterol Motil* 2019;**31**:e13615
- Wang L, An J, Song S, Mei M, Li W, Ding F, Liu S. Electroacupuncture preserves intestinal barrier integrity through modulating the gut microbiota in DSS-induced chronic colitis. *Life Sci* 2020;**261**:118473
- Segawa S, Fujiya M, Konishi H, Ueno N, Kobayashi N, Shigyo T, Kohgo Y. Probiotic-derived polyphosphate enhances the epithelial barrier function and maintains intestinal homeostasis through integrin-p38 MAPK pathway. *PLoS ONE* 2011;**6**:e23278
- Du SQ, Wang XR, Zhu W, Ye Y, Yang JW, Ma SM, Ji CS, Liu CZ. Acupuncture inhibits TXNIP-associated oxidative stress and inflammation to attenuate cognitive impairment in vascular dementia rats. *CNS Neurosci Ther* 2018;**24**:39–46
- Li JM, Yu R, Zhang LP, Wen SY, Wang SJ, Zhang XY, Xu Q, Kong LD. Dietary fructose-induced gut dysbiosis promotes mouse hippocampal neuroinflammation: a benefit of short-chain fatty acids. *Microbiome* 2019;**7**:98
- Wang S, Lin S, Zhu M, Li C, Chen S, Pu L, Lin J, Cao L, Zhang Y. Acupuncture reduces apoptosis of granulosa cells in rats with premature ovarian failure via restoring the PI3K/Akt signaling pathway. *Int J Mol Sci* 2019;**20**:6311
- Dou B, Li Y, Ma J, Xu Z, Fan W, Tian L, Chen Z, Li N, Gong Y, Lyu Z, Fang Y, Liu Y, Xu Y, Wang S, Chen B, Guo Y, Guo Y, Lin X. Role of neuroimmune crosstalk in mediating the anti-inflammatory and analgesic effects of acupuncture on inflammatory pain. *Front Neurosci* 2021;**15**:695670
- Tsai MJ, Hsu YL, Wang TN, Wu LY, Lien CT, Hung CH, Kuo PL, Huang MS. Aryl hydrocarbon receptor (AhR) agonists increase airway epithelial matrix metalloproteinase activity. *J Mol Med (Berl)* 2014;**92**:615–28
- Fasolino I, Izzo AA, Clavel T, Romano B, Haller D, Borrelli F. Orally administered allyl sulfides from garlic ameliorate murine colitis. *Mol Nutr Food Res* 2015;**59**:434–42

36. Zhang S, Xu W, Wang H, Cao M, Li M, Zhao J, Hu Y, Wang Y, Li S, Xie Y, Chen G, Liu R, Cheng Y, Xu Z, Zou K, Gong S, Geng L. Inhibition of CREB-mediated ZO-1 and activation of NF-kappaB-induced IL-6 by colonic epithelial MCT4 destroys intestinal barrier function. *Cell Prolif* 2019;**52**:e12673
37. Abdallah A, Elemba E, Zhong Q, Sun Z. Gastrointestinal interaction between dietary amino acids and gut microbiota: with special emphasis on host nutrition. *Curr Protein Pept Sci* 2020;**21**:785–98
38. Wang N, Jiang X, Zhang S, Zhu A, Yuan Y, Xu H, Lei J, Yan C. Structural basis of human monocarboxylate transporter 1 inhibition by anti-cancer drug candidates. *Cell* 2021;**184**:370.e13–83
39. Rajakovich LJ, Balskus EP. Metabolic functions of the human gut microbiota: the role of metalloenzymes. *Nat Prod Rep* 2019;**36**:593–625
40. Jan JS, Yang CH, Wang MH, Lin FL, Yen JL, Hsieh I, Khotimchenko M, Lee TH, Hsiao G. Hirsutanol A attenuates lipopolysaccharide-mediated matrix metalloproteinase 9 expression and cytokines production and improves endotoxemia-induced acute sickness behavior and acute lung injury. *Mar Drugs* 2019;**17**:360
41. Shiao ML, Yuan C, Crane AT, Voth JP, Juliano M, Stone LLH, Nan Z, Zhang Y, Kuzmin-Nichols N, Sanberg PR, Grande AW, Low WC. Immunomodulation with human umbilical cord blood stem cells ameliorates ischemic brain injury—a brain transcriptome profiling analysis. *Cell Transplant* 2019;**28**:864–73
42. Buisson A, Vazeille E, Minet-Quinard R, Goutte M, Bouvier D, Goutorbe F, Pereira B, Barnich N, Bommelaer G. Fecal matrix metalloproteinase-9 and lipocalin-2 as biomarkers in detecting endoscopic activity in patients with inflammatory bowel diseases. *J Clin Gastroenterol* 2018;**52**:e53–62
43. Maroni L, van de Graaf SF, Hohenester SD, Oude Elferink RP, Beuers U. Fucosyltransferase 2: a genetic risk factor for primary sclerosing cholangitis and Crohn's disease—a comprehensive review. *Clin Rev Allergy Immunol* 2015;**48**:182–91
44. Fletcher JR, Pike CM, Parsons RJ, Rivera AJ, Foley MH, McLaren MR, Montgomery SA, Theriot CM. *Clostridioides difficile* exploits toxin-mediated inflammation to alter the host nutritional landscape and exclude competitors from the gut microbiota. *Nat Commun* 2021;**12**:462
45. Norouzi Z, Salimi A, Halabian R, Fahimi H. Nisin, a potent bacteriocin and anti-bacterial peptide, attenuates expression of metastatic genes in colorectal cancer cell lines. *Microb Pathog* 2018;**123**:183–9
46. López-López N, González-Curiel I, Treviño-Santa Cruz MB, Rivas-Santiago B, Trujillo-Paez V, Enciso-Moreno JA, Serrano CJ. Expression and vitamin D-mediated regulation of matrix metalloproteinases (MMPs) and tissue inhibitors of metalloproteinases (TIMPs) in healthy skin and in diabetic foot ulcers. *Arch Dermatol Res* 2014;**306**:809–21
47. Sun CY, Young GH, Hsieh YT, Chen YH, Wu MS, Wu VC, Lee JH, Lee CC. Protein-bound uremic toxins induce tissue remodeling by targeting the EGF receptor. *J Am Soc Nephrol* 2015;**26**:281–90
48. Garcia VP, Rocha HNM, Silva GM, Amaral TAG, Secher NH, Nobrega ACL, Vianna LC, Rocha NG. Exogenous L-arginine reduces matrix metalloproteinase-2 and -9 activities and oxidative stress in patients with hypertension. *Life Sci* 2016;**157**:125–30
49. Kumar M, Sandhir R. Hydrogen sulfide attenuates hyperhomocysteinemia-induced blood-brain barrier permeability by inhibiting MMP-9. *Int J Neurosci* 2022;**132**:1061–71
50. Yan M, Zhao C, Lu S, Cui J, Sun Z, Liu X, Liu S, Huo Y, Yin S, Hu H. Trimethylamine N-oxide exacerbates acetaminophen-induced liver injury by interfering with macrophage-mediated liver regeneration. *J Cell Physiol* 2022;**237**:897–910
51. Steck N, Mueller K, Schemann M, Haller D. Bacterial proteases in IBD and IBS. *Gut* 2012;**61**:1610–8

(Received September 15, 2022, Accepted April 10, 2023)